Linear and Nonlinear Control of UAVs: Design and Experimental Validation

Luís Carlos Cunha Martins

luis.cunha.martins@tecnico.ulisboa.pt

Instituto Superior Técnico, Universidade de Lisboa, Lisboa, Portugal

June 2019

Abstract: This dissertation presents full control solutions for a quadrotor using linear and nonlinear methods. The dynamical model of the quadrotor is derived. Whereas the nonlinear controllers are designed considering this model, a linearization of the dynamics is required to synthesize the linear controllers. Linear Quadratic Regulator and Feedback Linearization were the techniques applied to tackle the control problem. Two control structures were devised using the linear approach and three different architectures, exploring the concepts of static and dynamic feedback, were developed for the nonlinear method. The capacity of trajectory tracking, in the presence of measurements noise, and the robustness to significant deviations of the mass and inertia values were evaluated in simulation. Thereby, the most promising linear and nonlinear solutions were selected for implementation in the actual quadrotor. The selected linear approach consists of an inner-outer loop control structure, where the innermost loop is responsible for the attitude control and the outermost solves the positioning control. In both loops, integrative action is incorporated. The second solution comprises a nonlinear inner loop that results from the application of static feedback linearization to the attitude and altitude dynamics. Linear quadratic controllers with integrative action are implemented not only to the resulting inner-loop chain of integrators, but also to the outer-loop, that controls the horizontal movement and, consequently, stabilizes the zero-dynamics. The required full state-feedback relies on measurements from motion sensors and on on-flight estimates provided by Kalman filters and an attitude filter. The selected control systems are implemented in a commercially available drone, equipped with an Inertial Measurement Unit, a compass and an altimeter. A motion capture system gives the inertial position of the drone. The results obtained allow the validation of the modeling and control system architectures.

Keywords: Control, Linear Quadratic Regulator, Feedback Linearization, Integrative Action, Trajectory Tracking

1. INTRODUCTION

In recent years, the popularity of drones has increased immensely as the embedded technology advanced. This growth translated into an intensive study of these Unmanned Aerial Vehicles. Its maneuverability, hovering capabilities, reduced price and small size not only enable the quadrotors to be equated in a wide range of applications, such as infrastructure inspection or area monitoring, but also constitute them as an excellent alternative for the experimentation of control and navigation techniques. At the core of the development of these applications, a robust control structure and an in-flight state-estimation is required.

The study of the control of quadrotors is vast and includes diverse linear and nonlinear techniques. Concerning the linear approaches, the majority of the bibliography reports the application of classical PIDs control and modern LQR controllers. In Bouabdallah et al. (2004) a comparison between the performances of the classical and the modern controllers referred, in simulation and in flight, for attitude control is established. This work evidences that the non-inclusion of an integrative action in LQR control for attitude originates a steady-state error. Bauer and Bokor (2008) implemented an LQ servo controller with a double integrator for trajectory tracking in simulation. Lastly, an inner and outer control loop with LQR control with integration action is proposed by Raja (2017). This control structure, designed for a model of a quadrotor obtained through Jacobian linearization, is successfully implemented in a UAV and enables a more effective attitude response.

Notwithstanding that various works attest the success of tackling the control problem with linear techniques, applying nonlinear control methods that consider a more comprehensive model of vehicle dynamics can lead to better performance. In the literature, it is possible to find a variety of nonlinear approaches applied to quadrotors. Within these methods, Feedback Linearization has attracted research interest throughout the years. Das et al. (2008) discussed a two-loop approach where, in the inner loop, responsible for altitude and attitude control, feedback linearization was applied and, in the outermost, proportional derivative controllers were used to control the horizontal movement. Additionally, in both loops, Sliding Mode control is included in order to deal more effectively

with disturbances. The simulation results validated the approach. Freddi et al. (2011) used feedback linearization to design a double loop control structure capable of performing not only trajectory tracking but also roll and pitch control in the event of a rotor failure. The simulation tests highlight this capacity of the fault tolerant controller proposed. A distinct two-loop architecture using feedback linearization is proposed by Wang et al. (2011). In this work, the attitude of the quadcopter only implicitly appears in the transformation matrix and is not a controlled state. The aerial vehicle proved to fly with good accuracy since the control errors obtained in hovering tests are within 3 cm for all Cartesian coordinates.

In this extended abstract, the linear and nonlinear control structures that attained better results in the simulation tests are presented. These control solutions were experimentally validated resorting to an off-the-shelf quadcopter. It is important to stress that three additional control schemes that are not addressed in this document were implemented and validated in simulation and are reported in the dissertation. A linearized model of the quadcopter is derived for the hover condition in order to enable the implementation of the linear controllers. The reconstruction of the state-variables that are not directly available through sensors, namely the velocity and the Euler angles, is performed resorting to Kalman Filters and an attitude filter, respectively. For the attitude filter, in the first proposed solution, the filter developed by Madgwick et al. (2011) is applied, whereas, in the second, the one devised by Madeiras et al. (2019) is used. Both control solutions possess an inner-outer loop structure, where the innermost loop is responsible for the attitude control, and the outermost solves the positioning control. In both loops an integrative action is present. The Linear Quadratic Regulator and Feedback Linearization methods are considered to tackle the control problem.

The main contributions of the work developed throughout the thesis are the derivation of a simplified dynamical model for quadrotors with X configuration, the subsequent linearization for a trim position, the application of model-based LQR control with integrative action considering two different structures, the study of three distinct control architectures that rely on the nonlinear technique Feedback Linearization and the experimental validation of a linear and a nonlinear control approaches.

This extended abstract is organized as follow: the physical model and the subsequent linearization are detailed in section 2; in section 3, the state-estimation is addressed; the theoretical basis of the control techniques considered are presented in section 4; the simulation results obtained with the simplified nonlinear model and the control structures, which are designed in section 5, are discussed in section 6; the quadcopter model and its sensors are detailed, and the implementation of the controllers is described in section 7; experimental results are presented and analyzed in section 8; finally, some concluding remarks are drawn.

2. PHYSICAL MODEL

2.1 Nonlinear Model

In this section, the nonlinear model of the UAV based on the Newton-Euler formalism is presented. The nonlinear dynamics are described in the body-fixed $\{B\}$ and in the inertial $\{I\}$ frames, depicted in Fig. 1. The unit vectors along the axis of the body-fixed frame are denoted by $\{\vec{b}_1, \vec{b}_2, \vec{b}_3\}$ and the unit vector along the inertial frame $\{I\}$ axis are denoted by $\{\vec{a}_1, \vec{a}_2, \vec{a}_3\}$. It is assumed that the origin of the body-fixed frame $\{B\}$ is coincident with the center of mass of the quadrotor.

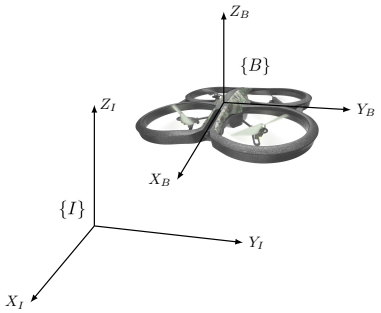

Fig. 1. Reference frames in which the nonlinear dynamics are described.

Let $\mathbf{p} = [x\ y\ z]^T$ denote the position vector of the center of mass of the UAV in the inertial frame. Let $\boldsymbol{\eta} = [\varphi\ \theta\ \psi]^T$ describe the orientation vector, in terms of Euler angles, of the body-fixed frame with respect to the inertial frame, where φ, θ and ψ are the roll, pitch and yaw angles, respectively. Let $\boldsymbol{\omega} = [p\,q\,r]^T$ represent the angular velocity described in the reference frame $\{B\}$. The rigid body equations of motion of the quadcopter according to Mahony et al. (2012) are given by:

$$m\ddot{\mathbf{p}} = -mg\vec{a}_3 + {}^I\mathbf{R}_B\mathbf{F} \tag{1}$$

$$\mathbf{I}\dot{\boldsymbol{\omega}} = -\boldsymbol{\omega} \times \mathbf{I}\boldsymbol{\omega} + \boldsymbol{\tau} \tag{2}$$

where $\mathbf{I}$ corresponds to the 3×3 constant inertia matrix described in the body fixed-frame, m is the total mass of the quadrotor, g denotes the gravity acceleration, $\mathbf{F}$ and $\boldsymbol{\tau}$ denote, respectively, the principal nonconservative forces and moments applied to the UAV airframe by the aerodynamics of the rotors, both described in the reference frame $\{B\}$, and ${}^I\mathbf{R}_B$ is the rotation matrix from the body-fixed to the inertial frame. The Euler angles follow the sequence of rotation Z-Y-X that is described in Oriolo et al. (2010). The resultant rotation matrix is given by:

$${}^I\mathbf{R}_B = \begin{bmatrix} c_\theta c_\psi & s_\varphi s_\theta c_\psi - c_\varphi s_\psi & c_\varphi s_\theta c_\psi + s_\varphi s_\psi \\ c_\theta s_\psi & s_\varphi s_\theta s_\psi - c_\varphi c_\psi & c_\varphi s_\theta s_\psi - s_\varphi c_\psi \\ -s_\theta & s_\varphi c_\theta & c_\varphi c_\theta \end{bmatrix} \tag{3}$$

where c and s are the shorthand forms for $\cos()$ and $\sin()$, respectively.

The angle rates $\dot{\boldsymbol{\eta}} = [\dot{\varphi}\ \ \dot{\theta}\ \ \dot{\psi}]^T$ are obtained from the body rotational rates using the following system of equations:

$$\begin{bmatrix} \dot{\varphi} \\ \dot{\theta} \\ \dot{\psi} \end{bmatrix} = \mathbf{T}(\boldsymbol{\eta})\,\boldsymbol{\omega} = \begin{bmatrix} 1 & \sin(\varphi)\tan(\theta) & \cos(\varphi)\tan(\theta) \\ 0 & \cos(\varphi) & -\sin(\varphi) \\ 0 & \sin(\varphi)\sec(\theta) & \cos(\varphi)\sec(\theta) \end{bmatrix} \begin{bmatrix} p \\ q \\ r \end{bmatrix} \tag{4}$$

According to Leishman (2000), the steady-state thrust T_i and yaw moment τ_{ψ_i} generated by a rotor in free air can be modeled as follow:

$$T_i = c_{T_i}\Omega_i^2 \tag{5}$$

$$\tau_{\psi_i} = c_{\tau_i}\Omega_i^2 \tag{6}$$

where c_{T_i} and c_{τ_i} are coefficients possible to determine experimentally that are dependent on the area of the disk,

the radius of the rotor, the density of air, the geometry and the profile of the rotor, and the effect of drag by the rotor flow, and Ω_i is the rotation speed of the rotor i. Therefore, the relation between the generated yaw moment τ_{ψ_i} by a rotor and its generated thrust T_i is described by the following expression:

$$\tau_{\psi_i} = \frac{c_{\tau_i}}{c_{T_i}} T_i = c_i T_i \tag{7}$$

The roll and pitch moments, τ_φ and τ_θ, result from the generated thrust of the rotor and its arrangement relative to the center of mass of the quadcopter. Hence, the resultant total thrust T and moments τ_φ, τ_θ and τ_ψ, for a quadrotor with a *X-configuration*, are computed through:

$$\begin{bmatrix} T \\ \tau_\varphi \\ \tau_\theta \\ \tau_\psi \end{bmatrix} = \begin{bmatrix} 1 & 1 & 1 & 1 \\ L & -L & -L & L \\ -L & -L & L & L \\ c_1 & -c_2 & c_3 & -c_4 \end{bmatrix} \begin{bmatrix} T_1 \\ T_2 \\ T_3 \\ T_4 \end{bmatrix} \tag{8}$$

where L denotes the perpendicular distance of the rotor to the x or y axis of the body-fixed frame, as the case may be.

There are various aerodynamic and gyroscopic effects associated with the rotors craft that increase the complexity of the model. However, a model with such level of precision is not required, not only because the control can overcome these secondary effects according to Mahony et al. (2012), but also due to the fact that is widely shown in the literature that the control can achieve high performance with the simplified model of the rotor. Consequently, high order effects such as *blade flapping*, *aerodynamic drag*, *translational lift* and *vortex states* caused by axial motion are neglected. Furthermore, it is assumed that the total thrust generated T is oriented along the $\vec{b}_3$ direction, i.e., parallel to the axis of the rotor, and the coefficients of the rotor are constant (static thrust and moments).

Moreover, the quadrotor is assumed to be exactly symmetrical, which implies that the inertia matrix is diagonal, and the rotor gyroscopic effects are neglected. Additionally, since the UAV flies at a height higher than $0,50m$, except when the take-off or the landing occurs, the ground effect is ignored.

Considering the equations previously defined and the approximations and assumptions described, let

$$\mathbf{x} = [x \;\; y \;\; z \;\; \varphi \;\; \theta \;\; \psi \;\; \dot{x} \;\; \dot{y} \;\; \dot{z} \;\; p \;\; q \;\; r]^T \tag{9}$$

denote the vector of state-variables and let

$$\mathbf{u} = [T \;\; \tau_\varphi \;\; \tau_\theta \;\; \tau_\psi]^T \tag{10}$$

represent the input vector, the quadcopter dynamics can be written in the compact form

$$\dot{\mathbf{x}} = \begin{bmatrix} \dot{\mathbf{p}} \\ \mathbf{T}(\boldsymbol{\eta})\,\boldsymbol{\omega} \\ -g\,\vec{a}_3 \\ \frac{I_y - I_z}{I_x} qr \\ \frac{I_z - I_x}{I_y} pr \\ \frac{I_x - I_y}{I_z} pq \end{bmatrix} + \begin{bmatrix} \mathbf{0}_{6\times1} & \mathbf{0}_{6\times3} \\ \frac{1}{m}\,{}^I\mathbf{R}_{B\,i3} & \mathbf{0}_{3\times3} \\ \mathbf{0}_{3\times1} & \mathbf{I}^{-1} \end{bmatrix} \mathbf{u} \tag{11}$$

with $i = 1, 2, 3$.

2.2 Linearized Model

The point of equilibrium for which the linearization will be deduced is the hover condition ($\mathbf{p} = [x \; y \; z]^T$, $\boldsymbol{\eta} = [0 \; 0 \; 0]^T$), where the yaw angle ψ is additionally considered zero. Note that the linearization could be performed for other conditions, however, this one was chosen given its simplicity. By resorting to the Taylor series till the first order term enables to approximate the cosine of the Euler angles to 1 and the sine and tangent of the referred angles to the angle itself.

For the *height subsystem*, the differential equation simplifies into:

$$\ddot{z} \simeq \frac{1}{m}(T - mg) \tag{12}$$

Defining the following state variables and modified input of the subsystem,

$$\mathbf{x_z} = [z \;\; \dot{z}]^T, \;\; \mathbf{u_z} = T - mg \tag{13}$$

leads to the state-space representation described below:

$$\dot{\mathbf{x}}_\mathbf{z} = \begin{bmatrix} 0 & 1 \\ 0 & 0 \end{bmatrix} \mathbf{x_z} + \begin{bmatrix} 0 \\ \frac{1}{m} \end{bmatrix} \mathbf{u_z} \tag{14}$$

$$\mathbf{y_z} = [1 \;\; 0]\,\mathbf{x_z} \tag{15}$$

The variation of the position of the UAV along the x and y directions of the inertial frame is a direct result of the variation of pitch and roll angles, respectively. The linearization of the second derivative of the pitch angle yields:

$$\ddot{\theta} \simeq \frac{\tau_\theta}{I_y} \tag{16}$$

Defining the consequent state variables and modified input of the subsystem,

$$\mathbf{x}_\theta = [\theta \;\; \dot{\theta}]^T, \;\; \mathbf{u}_\theta = \tau_\theta \tag{17}$$

results in the state-space representation described below:

$$\dot{\mathbf{x}}_\theta = \begin{bmatrix} 0 & 1 \\ 0 & 0 \end{bmatrix} \mathbf{x}_\theta + \begin{bmatrix} 0 \\ \frac{1}{I_y} \end{bmatrix} \mathbf{u}_\theta \tag{18}$$

$$\mathbf{y}_\theta = [1 \;\; 0]\,\mathbf{x}_\theta \tag{19}$$

The linearization of the second derivative of the roll angle results in:

$$\ddot{\varphi} \simeq \frac{\tau_\varphi}{I_x} \tag{20}$$

Letting the following equations define the state variables and modified input of the subsystem

$$\mathbf{x}_\varphi = [\varphi \;\; \dot{\varphi}]^T, \;\; \mathbf{u}_\varphi = \tau_\varphi \tag{21}$$

the obtained state-space representation is described by

$$\dot{\mathbf{x}}_\varphi = \begin{bmatrix} 0 & 1 \\ 0 & 0 \end{bmatrix} \mathbf{x}_\varphi + \begin{bmatrix} 0 \\ \frac{1}{I_x} \end{bmatrix} \mathbf{u}_\varphi \tag{22}$$

$$\mathbf{y}_\varphi = [1 \;\; 0]\,\mathbf{x}_\varphi \tag{23}$$

The acceleration in the body-fixed frame vector, ${}^B\mathbf{a}$, is given by

$${}^B\mathbf{a} = \frac{\mathbf{F}}{m} - {}^B\mathbf{R}_I g\vec{a_3} - \boldsymbol{\omega} \times {}^B\mathbf{v} \tag{24}$$

where ${}^B\mathbf{v}$ denotes the velocities in the body-fixed frame and the term $\boldsymbol{\omega} \times {}^B\mathbf{v}$ corresponds to the centripetal acceleration. The accelerations along the x axis, ${}^B\mathbf{a}_x$, and along the y axis, ${}^B\mathbf{a}_y$, of the body-fixed frame, after being linearized and assuming that the yaw angle ψ is kept at zero and that the movement along the body fixed-frame

x and y directions occurs with negligible variations along the z direction, are equal to

$$^{B}\mathbf{a}_x = \theta g \tag{25}$$

$$^{B}\mathbf{a}_y = -\varphi g \tag{26}$$

Noticing that the forward velocity of the UAV in the body-fixed frame, u, is the integral of $^{B}\mathbf{a}_x$, and the sideway velocity, v, is the integral of $^{B}\mathbf{a}_y$, equations (25) and (26) can be rewritten as

$$\dot{u} = \theta g \tag{27}$$

$$\dot{v} = -\varphi g \tag{28}$$

With the establishment of the next state-variables and modified input of the subsystem:

$$\mathbf{x_x} = [^{B}x_I \ u]^T, \ \mathbf{u_x} = \theta \tag{29}$$

where $^{B}x_I$ denotes the x coordinate of the inertial position described according to the orientation of the body-fixed frame, the following state-space representation, that relates the $^{B}x_I$ coordinate of the position with the pitch angle, θ, is obtained

$$\dot{\mathbf{x}}_\mathbf{x} = \begin{bmatrix} 0 & 1 \\ 0 & 0 \end{bmatrix} \mathbf{x_x} + \begin{bmatrix} 0 \\ g \end{bmatrix} \mathbf{u_x} \tag{30}$$

$$\mathbf{y_x} = [1 \ 0] \, \mathbf{x_x} \tag{31}$$

By defining the following state-variables and modified input of the subsystem:

$$\mathbf{x_y} = [^{B}y_I \ v]^T, \ \mathbf{u_y} = \varphi \tag{32}$$

where $^{B}y_I$ denotes the y coordinate of the inertial position described according to the orientation of the body-fixed, the following state-space representation, that relates this coordinate of the position with the roll angle, φ, is obtained

$$\dot{\mathbf{x}}_\mathbf{y} = \begin{bmatrix} 0 & 1 \\ 0 & 0 \end{bmatrix} \mathbf{x_y} + \begin{bmatrix} 0 \\ -g \end{bmatrix} \mathbf{u_y} \tag{33}$$

$$\mathbf{y_y} = [1 \ 0] \, \mathbf{x_y} \tag{34}$$

The linearization of the second derivative of the yaw angle yields:

$$\ddot{\psi} \simeq \frac{\tau_\psi}{I_z} \tag{35}$$

Letting the state-variables and entry of the subsystem be described by

$$\mathbf{x}_\psi = [\psi \ \dot{\psi}]^T, \ \mathbf{u}_\psi = \tau_\psi \tag{36}$$

enables the following state-space representation

$$\dot{\mathbf{x}}_\psi = \begin{bmatrix} 0 & 1 \\ 0 & 0 \end{bmatrix} \mathbf{x}_\psi + \begin{bmatrix} 0 \\ \dfrac{1}{I_z} \end{bmatrix} \mathbf{u}_\psi \tag{37}$$

$$\mathbf{y}_\psi = [1 \ 0] \, \mathbf{x}_\psi \tag{38}$$

3. STATE-ESTIMATION

3.1 Attitude Filter

Magdwick Attitude Filter The Kalman filter is widely used for sensor fusion to estimate the attitude, however, for practical reasons, the orientation filter developed by Madgwick et al. (2011) was opted and applied in the first solution. The computation is performed using the quaternion representation and fuses the measurements of the gyroscope, accelerometer and magnetometer through an optimized gradient-descent algorithm.

Nonlinear Attitude Filter The attitude filter considered in the second solution, developed by João Madeiras Madeiras et al. (2019), is a nonlinear filter that fuses the accelerometer and gyroscope measurements. The gains of this attitude complementary filter can be computed considering a linear system that is obtained resorting to a Lyapunov transformation. Furthermore, this filter is proved to be uniformly asymptotically stable assuming a bounded pitch angle ($|\theta| < \pi/2$).

3.2 Kalman Filter

This filter, with a statistical basis, constitutes a solution to optimal stochastic estimation for linear systems and aims the minimization of the estimation mean squared error, under the assumptions of zero-mean Gaussian process and sensor noises, ϑ and ν, respectively, as proposed by Kalman (1960). For the estimation of the velocities the following observable subsystem with noise disturbances was considered:

$$\dot{\mathbf{x}} = \begin{bmatrix} 0 & 1 \\ 0 & 0 \end{bmatrix} \mathbf{x} + \vartheta \tag{39}$$

$$\mathbf{y} = [1 \ 0] \, \mathbf{x} + \nu \tag{40}$$

where the first state-variable is one of the inertial coordinates (x, y, z), whose measurements are available through sensors, and the second state-variable is the respective inertial velocity $(\dot{x}, \dot{y}, \dot{z})$. The estimates for the body-fixed velocities u and v are obtained by applying the following rotation:

$$\begin{bmatrix} \hat{u} \\ \hat{v} \end{bmatrix} = {}^{B}\mathbf{R}_{I_{ij}} \begin{bmatrix} \hat{\dot{x}} \\ \hat{\dot{y}} \\ \hat{\dot{z}} \end{bmatrix}, \ i \in \{1, 2\}, j \in \{1, 2, 3\} \tag{41}$$

4. CONTROL THEORY

4.1 Linear Quadratic Regulator with Integrative Action

The Linear Quadratic Regulator is an optimal controller that uses full state-feedback and is derived as a solution to an optimization process where the systems dynamics imposes the restrictions. For a system described by the state-space representation

$$\dot{\mathbf{x}} = \mathbf{A}\mathbf{x} + \mathbf{B}\mathbf{u} \tag{42}$$

$$\dot{\mathbf{y}} = \mathbf{C}\mathbf{x} + \mathbf{D}\mathbf{u} \tag{43}$$

the optimal regulator problem determines the gain matrix K, constituent of the optimal control vector

$$\mathbf{u}(t) = -\mathbf{K}\mathbf{x}(t) \tag{44}$$

that ensures the minimization of the performance index

$$J = \int_0^\infty (\mathbf{x}^T\mathbf{Q}\mathbf{x} + \mathbf{u}^T\mathbf{R}\mathbf{u})dt \tag{45}$$

where the first quadratic form includes the real symmetric state weighting matrix $\mathbf{Q}$ and the second quadratic term comprises the real symmetric control weighting matrix $\mathbf{R}$.

The computation of the optimal gains is performed through:

$$\mathbf{K} = \mathbf{R}^{-1}\mathbf{B}^T\mathbf{P} \tag{46}$$

where the positive-definite matrix $\mathbf{P}$ results from the steady-state Riccati equation:

$$\mathbf{A}^T\mathbf{P} + \mathbf{P}\mathbf{A} - \mathbf{P}\mathbf{B}\mathbf{R}^{-1}\mathbf{B}^T\mathbf{P} + \mathbf{Q} = \mathbf{0} \tag{47}$$

As a way of dealing with the effect of perturbations and with the steady-state error, an integrator was embedded in the control structure. This inclusion leads to

additional robustness of the control system and eliminates the steady-state errors due to constant disturbances. Let the reference signal be represented by $\mathbf{r}$ and the difference between the output of the system, $\mathbf{y}$, and the reference, $\mathbf{r}$, be the time derivative of the state-space variable that results from adding the referred integrator, ξ. The matrices of the resulting regulator are given by

$$\bar{\mathbf{A}} = \begin{bmatrix} \mathbf{A} & \mathbf{0} \\ -\mathbf{C} & \mathbf{0} \end{bmatrix}, \; \bar{\mathbf{B}} = \begin{bmatrix} \mathbf{B} \\ \mathbf{0} \end{bmatrix} \tag{48}$$

The optimal gains are computed by directly applying the LQR gain computation presented formerly. The optimal gain matrix obtained

$$\bar{\mathbf{K}} = [\mathbf{K} \; -\mathbf{k_1}] \tag{49}$$

is constituted by the vector of gains for the state-variables, $\mathbf{K}$, and by the gain for the integrative action, $\mathbf{k_1}$.

4.2 Feedback Linearization

Feedback Linearization consists in a nonlinear control approach that aims to algebraically transform nonlinear dynamics of systems, through nonlinear change of coordinates and nonlinear state feedback, into a model that is linear in the new set of coordinates. The linear model produced is an exact representation of the original nonlinear model over a large set of operating points (Henson and Seborg (1997)).

Given a nonlinear system of the form:

$$\mathbf{x} = \mathbf{f}(\mathbf{x}) + \mathbf{g}(\mathbf{x})\,\mathbf{u} \tag{50}$$

$$\mathbf{y} = \mathbf{h}(\mathbf{x}) \tag{51}$$

where $\mathbf{f}(\mathbf{x})$ and $\mathbf{h}(\mathbf{x})$ are, respectively, n and m-dimensional vectors of sufficiently smooth nonlinear functions and $\mathbf{g}(\mathbf{x})$ is an $(\mathrm{n} \times \mathrm{m})$-dimensional matrix of sufficiently smooth nonlinear functions. According to Vepa (2017), if the sum of the relative degrees $\mathbf{r}_j$ of each output $\mathbf{y}_j$ equals the number of state-variables, the system can be modified into a fully linear and decoupled controllable system through the application of the following transformation for each output $\mathbf{y}_j$:

$$\boldsymbol{\xi}_{j,1} = \mathbf{y}_j \tag{52}$$

$$\vdots$$

$$\boldsymbol{\xi}_{j,r_j} = \dot{\boldsymbol{\xi}}_{j,r_j-1} = \mathcal{L}_{\mathbf{f}}^{\mathbf{r_j}-\mathbf{1}}\mathbf{h}_j(\mathbf{x}) \tag{53}$$

$$\dot{\boldsymbol{\xi}}_{j,r_j} = \mathcal{L}_{\mathbf{f}}^{\mathbf{r_j}}\mathbf{h}_j(\mathbf{x}) + \sum_{i=1}^{m} \mathcal{L}_{\mathbf{g}_i}\mathcal{L}_{\mathbf{f}}^{\mathbf{r_j}-\mathbf{1}}\mathbf{h}_j(\mathbf{x})\mathbf{u}_i \tag{54}$$

where $\mathcal{L}$ represents the Lie Derivative, and of the next nonlinear static state feedback control law

$$\mathbf{u} = -\boldsymbol{\Lambda}^{-1}(\mathbf{x})\,\mathbf{b}(\mathbf{x}) + \boldsymbol{\Lambda}^{-1}(\mathbf{x})\,\mathbf{v} \tag{55}$$

where $\mathbf{v}$ is the transformed input variables vector, the *decoupling matrix* $\boldsymbol{\Lambda}(\mathbf{x})$ is defined as

$$\boldsymbol{\Lambda}(\mathbf{x}) = \begin{bmatrix} \mathcal{L}_{\mathbf{g}_1}\mathcal{L}_{\mathbf{f}}^{\mathbf{r_1}-\mathbf{1}}\mathbf{h}_1(\mathbf{x}) & \cdots & \mathcal{L}_{\mathbf{g}_\mathrm{m}}\mathcal{L}_{\mathbf{f}}^{\mathbf{r_1}-\mathbf{1}}\mathbf{h}_1(\mathbf{x}) \\ \vdots & \ddots & \vdots \\ \mathcal{L}_{\mathbf{g}_1}\mathcal{L}_{\mathbf{f}}^{\mathbf{r_m}-\mathbf{1}}\mathbf{h}_\mathrm{m}(\mathbf{x}) & \cdots & \mathcal{L}_{\mathbf{g}_\mathrm{m}}\mathcal{L}_{\mathbf{f}}^{\mathbf{r_m}-\mathbf{1}}\mathbf{h}_\mathrm{m}(\mathbf{x}) \end{bmatrix} \tag{56}$$

and $\mathbf{b}(\mathbf{x})$ is given by

$$\mathbf{b}(\mathbf{x}) = \begin{bmatrix} \mathcal{L}_{\mathbf{f}}^{\mathbf{r_1}}\mathbf{h}_1(\mathbf{x}) \\ \vdots \\ \mathcal{L}_{\mathbf{f}}^{\mathbf{r_m}}\mathbf{h}_\mathrm{m}(\mathbf{x}) \end{bmatrix} \tag{57}$$

It is clear that the *decoupling matrix* is required to be nonsingular.

After applying the input-output feedback linearization, the input-output model is linear in the new set of coordinates and is formed by a set of m chains of r_j integrators. Therefore, once each system is in linear and controllable form, is possible to stabilize these systems by means of linear controllers.

5. CONTROL DESIGN

5.1 Linear Quadratic Regulator with Integrative Action

The LQR with integrative action is applied for each subsystem present in the outer (position control) and in the inner (attitude control) loops. The control structure is schematized in Fig. 2, from which it is noted that the references for the pitch θ and roll φ angles result from the position control.

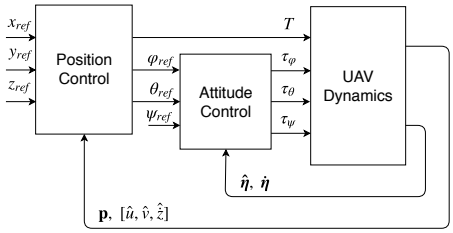

Fig. 2. Scheme of the inner-outer loop control structure implemented.

5.2 Feedback Linearization

The approach using feedback linearization control consists in applying it to the inner loop dynamics, formed by the attitude and altitude equations, and in stabilizing the outer loop with linear controllers. The zero-dynamics in this case will correspond to the horizontal movement dynamics. Let $\mathbf{y_{in}} = [z \;\; \varphi \;\; \theta \;\; \psi]^T$ define the output vector of the inner loop, $\mathbf{x_{in}}$ denote the vector of state-variables of the inner dynamics

$$\mathbf{x_{in}} = [z \;\; \dot{z} \;\; \varphi \;\; \theta \;\; \psi \;\; p \;\; q \;\; r]^T \tag{58}$$

and $\mathbf{u_{in}}$ describe the vector of inputs of the system

$$\mathbf{u_{in}} = [T \;\; \tau_\varphi \;\; \tau_\theta \;\; \tau_\psi]^T \tag{59}$$

Since the altitude and attitude dynamics combined have a total of 8 state-variables and $\sum_{j=1}^{4} r_j = 8$, the feedback linearization can be performed through a static state feedback law. The *decoupling matrix* $\boldsymbol{\Lambda}(\mathbf{x_{in}})$ of the nonlinear static state-feedback control law is defined by

$$\boldsymbol{\Lambda}(\mathbf{x_{in}}) = \begin{bmatrix} \dfrac{c_\theta\, c_\varphi}{m} & 0 & 0 & 0 \\ 0 & \dfrac{1}{I_x} & \dfrac{t_\theta\, s_\varphi}{I_y} & \dfrac{c_\varphi\, t_\theta}{I_z} \\ 0 & 0 & \dfrac{c_\varphi}{I_y} & -\dfrac{s_\varphi}{I_z} \\ 0 & 0 & \dfrac{s_\varphi}{I_y\, c_\theta} & \dfrac{c_\varphi}{I_z\, c_\theta} \end{bmatrix} \tag{60}$$

where t is shorthand form for tangent. The determinant of the preceding matrix is

$$\det(\boldsymbol{\Lambda}(\mathbf{x_{in}})) = \frac{\cos(\varphi)}{I_x\, I_y\, I_z\, m} \tag{61}$$

Thus, the *decoupling matrix* $\boldsymbol{\Lambda}(\mathbf{x_{in}})$ is invertible at any point defined by $|\varphi| < \frac{\pi}{2}$. Additionally, it is required

that $|\theta| < \frac{\pi}{2}$. The vector $\mathbf{b}(\mathbf{x_{in}})$ is directly obtained by extracting the terms that are independent of the input from the second derivatives of each output $\mathbf{y_{in}}_j$. Applying the transformation described from (52) to (54) for each output $\mathbf{y}_j$ yields the vector of transformed state-variables:

$$\boldsymbol{\xi}_{\mathbf{in}} = \begin{bmatrix} z & \dot{z} & \varphi & \dot{\varphi} & \theta & \dot{\theta} & \psi & \dot{\psi} \end{bmatrix}^T \tag{62}$$

As a result of the static state feedback control law and of the change of coordinates, the inner dynamics are now linearized and decoupled. These dynamics are translated into four single-input single-output chains of two integrators. Given the linear, decoupled and controllable form of the inner-loop dynamics, the Linear Quadratic Regulator control technique can be employed to each sequence. In each chain, an additional integrator was embedded into the feedback control to obtain additional robustness.

In fact, the *zero dynamics* are unstable. Therefore, an outer position control loop is necessary. The control strategy for this loop relies on LQR controllers with integrative action identical to the ones considered in the linear approach. The nonlinear control strategy is schematized in Fig. 3.

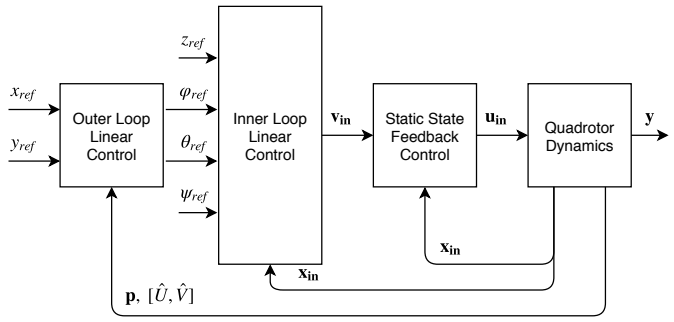

Fig. 3. Scheme of the static feedback linearization with zero-dynamics stabilization implemented.

6. SIMULATION

Concerning the design parameters, it is intended to control the position of the UAV while focusing in obtain responses with a settling time inferior to 6 seconds, with a maximum overshoot and oscillation inferior to 2 % and without static error. Regarding the rotational responses, since they are responsible for the stabilization of the quadcopter, a faster response, in furtherance of coping with the references that result from the translational control in the x and y directions of the inertial frame, is required. Therefore, the pitch and roll subsystems must necessarily present step responses with a settling time inferior to 1 second and fulfill the formerly defined overshoot, oscillation and error requirements. Considering the yaw subsystem, once it does not present such an important role in the stabilization of the drone as the other Euler angles, its response is not required to have this settling time. Therefore, for this Euler angle, the aim is a settling time inferior to 3 seconds and the already defined null static-error and overshoot and oscillation inferior to 2%. The control gains were obtained by analyzing the characteristics of the resulting step-responses. The **Q** and **R** matrices used in the linear and in the nonlinear control solutions are detailed, respectively, in Table. 1 and Table. 2.

Table 1. **Q** and **R** matrices used in the optimal gains computation for each subsystem of the linear control approach.

Subsystem	**Q**	**R**
Roll	$\mathrm{diag}(25, 1, 1500)$	200
Pitch	$\mathrm{diag}(25, 1, 1500)$	200
Yaw	$\mathrm{diag}(7, 1, 15)$	1
Height	$\mathrm{diag}(5, 1, 3)$	3
X Position	$\mathrm{diag}(15, 1, 10)$	1000
Y Position	$\mathrm{diag}(15, 1, 10)$	1000

Table 2. **Q** and **R** matrices used in the optimal gains computation for each subsystem of the nonlinear control approach.

Subsystem	**Q**	**R**
Roll	$\mathrm{diag}(6 \times 10^4, 7.5 \times 10^2, 2 \times 10^6)$	1
Pitch	$\mathrm{diag}(6 \times 10^4, 7.5 \times 10^2, 2 \times 10^6)$	1
Yaw	$\mathrm{diag}(7.5 \times 10^3, 20, 2 \times 10^5)$	1
Height	$\mathrm{diag}(15, 1, 15)$	1
X Inertial	$\mathrm{diag}(5, 1, 30)$	2×10^3
Y Inertial	$\mathrm{diag}(5, 1, 30)$	2×10^3

To ascertain the robustness of the proposed controllers and its model dependency, the impact of considering inaccurate values of the mass and the inertia of the quadcopter is studied. To this end, variations of 50% in the mass combined with decreases of 75% and increases of 300% in the inertia were studied. The references for the position are steps with an amplitude of 3 m and the reference for the yaw angle is a ramp with a slope of $0.1\,\mathrm{rad} \cdot \mathrm{s}^{-1}$.

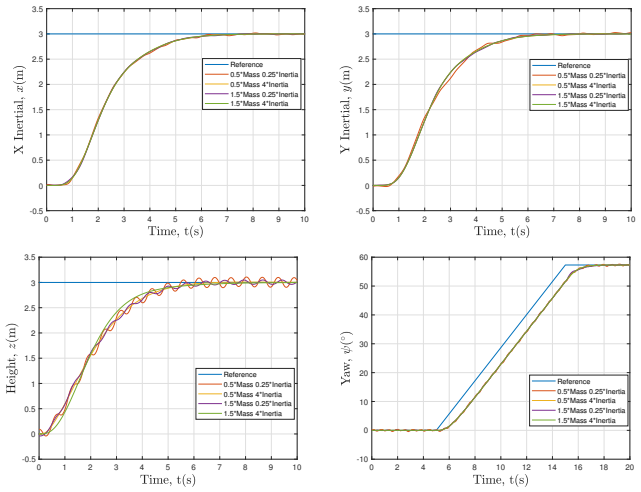

Fig. 4. Responses obtained with the linear approach in the robustness test. From left to right, top to bottom: (a) X Inertial; (b) Y Inertial; (c) Height; (d) Yaw.

The responses obtained with the model parameters variation with the linear approach are displayed in Fig. 4. It is visible that the step responses of the inertial coordinates x and y altered slightly. On the other hand, the height and yaw responses present an oscillatory behavior, characteristic of a marginally stable system, when a decrease of 75% is considered for the inertia matrix values.

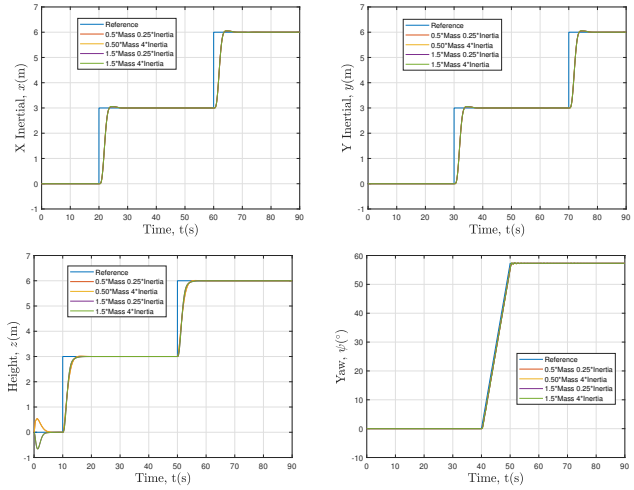

Fig. 5. Responses obtained with the nonlinear approach in the robustness test. From left to right, top to bottom: (a) X Inertial; (b) Y Inertial; (c) Height; (d) Yaw.

The position and yaw angle responses obtained in the model parameters variation test with the nonlinear control architecture are depicted in Fig. 5. These are very promising and important results since the performance did not deteriorate significantly even tough significant changes in the model parameters were consider and the amplitude of the steps required very aggressive responses. Compared to the results obtained for the same variations with the linear control, the static feedback linearization applied to the altitude and attitude dynamics achieved better results. Not only the responses remained stable, but also the control performance presented a higher consistency throughout the tests, which is reflected in the fact that all responses respected the design criteria.

To evaluate the performances of the proposed control architectures, a trajectory was created and given as a reference. Additionally, noise disturbances, modeled as zero-mean Gaussian white noise, were included to study the impact of the noise of the sensors. This trajectory is defined with a constant yaw angle equal to zero and, excluding the take-off, is formed by rectilinear sections, with a constant velocity of $0.05\,\mathrm{m}\cdot\mathrm{s}^{-1}$, and semicircular sections, with a constant angular velocity of $0.05\pi\,\mathrm{rad}\cdot\mathrm{s}^{-1}$.

From the observation of the Fig. 6, it can be concluded that the control structures implemented allow a good following of the trajectory. The time responses have a steady-state error for references with constant velocity, which was predictable since the integrator included in the control structure only has the capacity to eliminate the steady-state error for constant references. Notwithstanding, once the ramp references are followed up by constant references, the responses converge without error to the desired coordinate. Concerning the time response of the yaw angle, it is noticeable that the objective was achieved with both control solutions.

7. IMPLEMENTATION

The Parrot AR. Drone 2.0 was selected as the unmanned aerial vehicle used for testing the proposed control system solution. This commercially available quadcopter possesses an inboard Inertial Measurement Unit and a

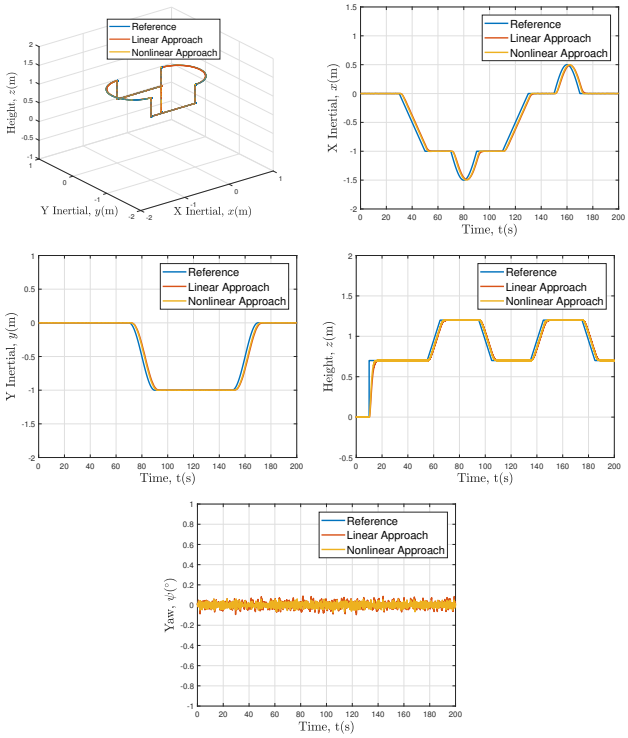

Fig. 6. Responses obtained during trajectory tracking in simulation with the two control approaches developed. From left to right, top to bottom: (a) Trajectory Tracking in 3D space; (b) X Inertial; (c) Y Inertial; (d) Height and (e) Yaw.

sonar board. The IMU is constituted by a 3-axis accelerometer, a 3-axis gyroscope and a barometric pressure sensor. The sonar board is equipped with two ultrasonic transducers and a 3-axis Compass. These sensors provide measurements of the acceleration, of the angular velocities, of the UAVs height and of the magnetic field. The inertial position of the vehicle is provided by a motion capture system.

In order to implement the control structure in the quadrotor, the "AR Drone 2.0 Quadcopter Embedded Coder" developed by Lee (2016) was used. This *Simulink* project enables direct access to the sensors and the actuators of the quadcopter.

The Pulse Width Modulation Commands for the actuators are computed from the Thrust and Moments, that result from the control law, through experimentally determined relations. The relevant physical quantities of this quadcopter are detailed in Table. 3

Table 3. Important physical quantities of the AR Drone 2.0.

L (m)	m (kg)	I_x (kg · m^2)	I_y (kg · m^2)	I_z (kg · m^2)
0.127	0.460	2.24×10^{-3}	2.90×10^{-3}	5.30×10^{-3}

8. EXPERIMENTAL RESULTS

8.1 Linear Solution

The experimental results obtained with the linear control scheme are depicted in Fig. 7. The trajectory tested is equal to the simulated one and it is possible to verify a

good tracking by the quadrotor. It is important to stress that: the take-off is present in the results depicted, the altimeter does not measure heights inferior to 30 cm and that a heavier battery was used leading to higher values of thrust. Nonetheless, despite this change in the total mass of the UAV, the results did not deteriorate since the integral action was included. For attitude estimation, the attitude filter proposed by Madgwick et al. (2011) was implemented in this approach.The controllers had to be adjusted when implemented in the UAV. The matrices **Q** and **R** used in this adjustment are detailed in Table. 4.

Table 4. **Q** and **R** matrices used in the adjustment of the controllers of the linear control approach implemented in the UAV.

Subsystem	**Q**	**R**
Yaw	diag(18, 2, 2)	30
X Position	diag(3, 1, 2)	300
Y Position	diag(3, 1, 2)	500
Height	diag(3, 1, 1)	1

By comparing the UAV results with the simulation responses, the similarities between them are clear, which indicates that the nonlinear model considered possesses a satisfactory degree of proximity. The histograms of the absolute error for the inertial coordinates and the yaw angle during the tracking of the trajectory (initiates at 20 seconds) are presented in Fig. 8. Even though the deviations are larger in the real system, they are still considered reduced. The local maxima visible in the position histograms are a consequence of the static error in the following of ramp inputs. Nevertheless, the maximum instances of error for all of these coordinates correspond approximately to zero, which is symptomatic of the capacity of the control system to maintain these coordinates at a constant value. The inertial coordinate x presented the higher deviations, which was expected since that was the subsystem more solicited. The values of the yaw angle obtained demonstrate that the goal defined for this Euler angle was achieved.

Table 5. Root-mean-square error obtained in simulation and in the experimental test with the selected linear control approach.

	x (m)	y (m)	z (m)	ψ (°)
Simulation	0.0865	0.0714	0.0556	0.0295
Experimental	0.1010	0.0781	0.0570	0.2244

The root-mean-square error for the trajectory tracking in simulation an in the real system is detailed in Table. 5. The height response obtained with the quadrotor has almost the same error obtained in simulation, whereas the other subsystems showed a forecastable increase in the real system due to the discarding of the higher order dynamics effects. In general, the errors were kept under reasonable values with the transition to the drone.

8.2 Nonlinear Solution

Implementing the static feedback linearization with zero-dynamics stabilization led to the experimental results depicted in Fig. 9. It is possible to note that this approach achieved a successful tracking of the predefined trajectory. Similar to the linear control results, the take-off is displayed as well, the previously referred saturation

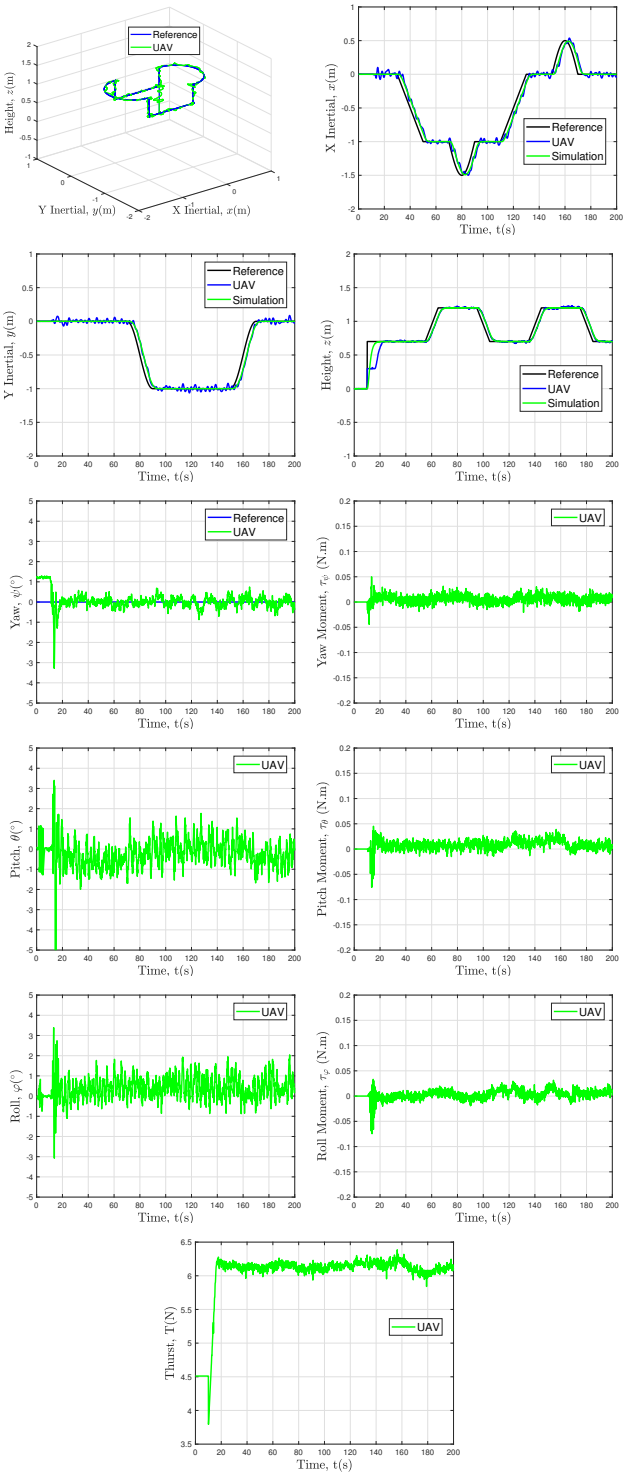

Fig. 7. Responses and actuations obtained with the UAV during trajectory tracking with the proposed linear control approach. From left to right, top to bottom: (a) Trajectory Tracking in 3D space; (b) X Inertial; (c) Y Inertial; (d) Height (e) Yaw; (f) Yaw Moment; (g) Pitch; (h) Pitch Moment; (i) Roll; (j) Roll Moment and (k) Thrust.

of the altimeter measurements is also evident and similarities between the experimental and the simulation results are noticeable, demonstrating once more the proximity between the nonlinear model developed and the actual

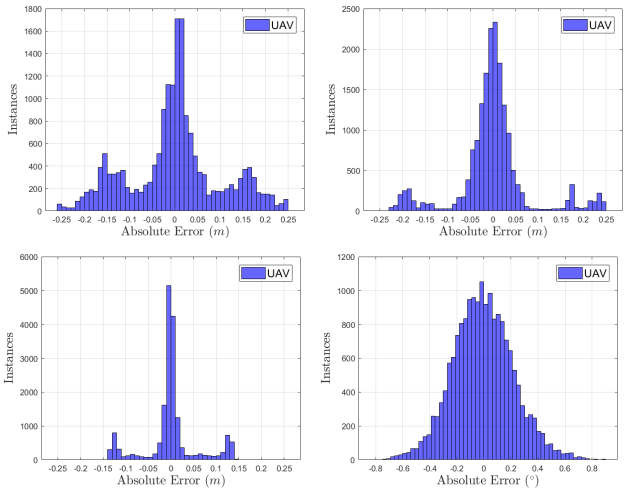

Fig. 8. Absolute error histograms obtained with the proposed linear control approach in the experimental test. Left to right, top to bottom: (a) X Inertial; (b) Y Inertial; (c) Height and (d) Yaw.

system. For attitude estimation, the nonlinear attitude filter proposed by Madeiras et al. (2019) was used in this approach. Identically to the former implementation, the controllers had to be adjusted when transitioning to the actual quadrotor. The matrices **Q** and **R** used in this adjustment are detailed in Table. 6.

Table 6. **Q** and **R** matrices used in the adjustment of the controllers of the selected nonlinear control approach implemented in the UAV.

Subsystem	**Q**	**R**
Roll	$\text{diag}(7.5\times10^3, 20, 2\times10^5)$	1
Pitch	$\text{diag}(7.5\times10^3, 20, 2\times10^5)$	1
Yaw	$\text{diag}(7.5\times10^3, 50, 1\times10^5)$	1
X Position	$\text{diag}(5, 1\times10^{-3}, 40)$	2×10^3
Y Position	$\text{diag}(5, 1\times10^{-3}, 40)$	2×10^3

The root-mean-square error for the trajectory tracking in simulation an in the real system obtained with the nonlinear control approach is detailed in Table. 7. Compared to the linear control implemented, it is noticeable that the error decreased with the application of the static feedback linearization technique to the altitude and attitude dynamics. Furthermore, this nonlinear method enabled achieving experimental results more proximate to the simulation. The improvement achieved with the nonlinear control is partly due to the faster position responses, which has as a consequence lower steady-state error in the following of ramp inputs.

Table 7. Root-mean-square error obtained in simulation and in the experimental test with the selected nonlinear control approach.

	x (m)	y (m)	z (m)	ψ (°)
Simulation	0.0632	0.0482	0.0385	0.0223
Experimental	0.0666	0.0518	0.0394	0.1715

By analyzing the histograms of the absolute error for the inertial coordinates and the yaw angle during the tracking trajectory (initiates at 20 seconds) displayed in Fig. 10, it is noted that a higher number of approximately zero absolute error instances was obtained with the second

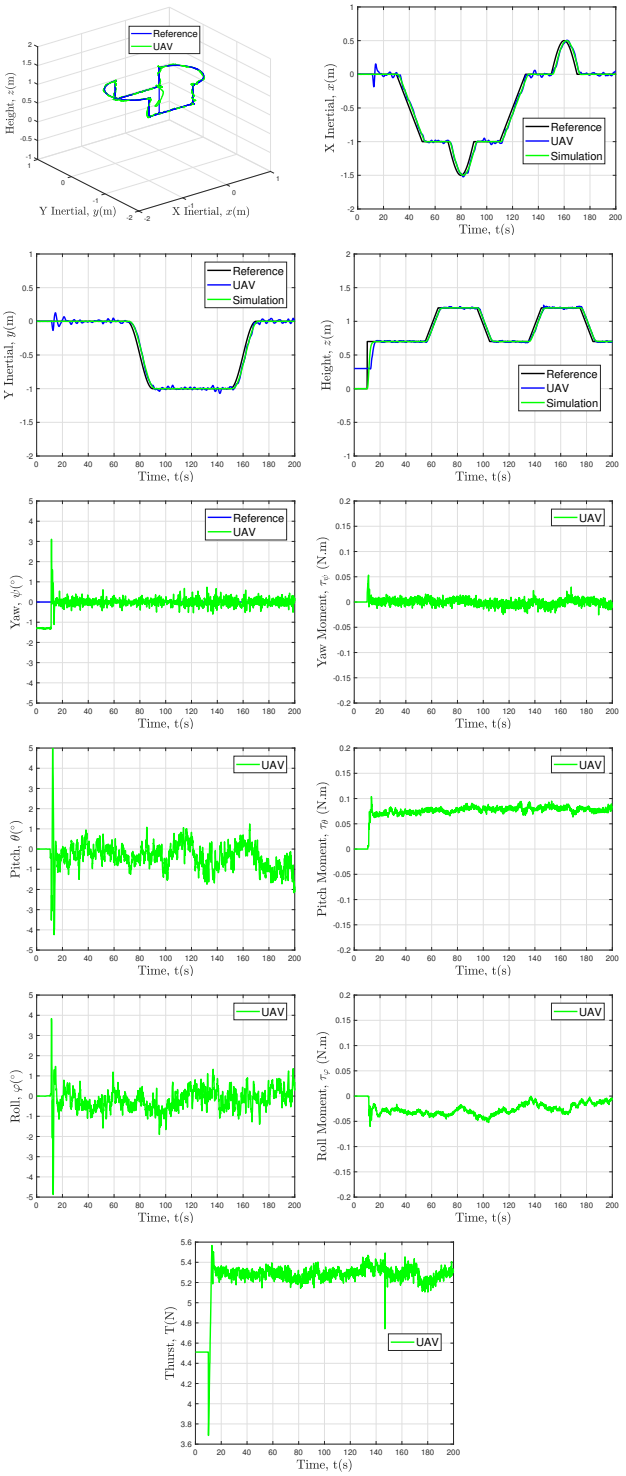

Fig. 9. Responses and actuations obtained with the UAV during trajectory tracking with the proposed nonlinear control approach. From left to right, top to bottom: (a) Trajectory Tracking in 3D space; (b) X Inertial; (c) Y Inertial; (d) Height (e) Yaw; (f) Yaw Moment; (g) Pitch; (h) Pitch Moment; (i) Roll; (j) Roll Moment and (k) Thrust.

control approach implemented. Moreover, as a result of presenting faster responses, this approach has the local maxima of the histograms closer to zero than the previous control structure considered. Analogously to the inner-

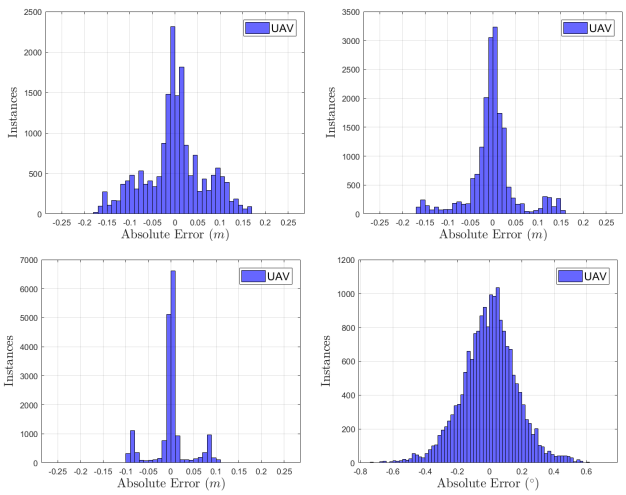

Fig. 10. Absolute error histograms obtained with the proposed nonlinear control approach in the experimental test. Left to right, top to bottom: (a) X Inertial; (b) Y Inertial; (c) Height and (d) Yaw.

outer control using LQR with integrative action, the response with more deviations is the inertial coordinate x and the one with less is the height, which is the affected at the smallest scale by unmodelled high-order effects. Overall, the implementation of the static feedback linearization in the inner-loop improved the tracking performance of the control structure by not only attaining the objectives but also leading to better results.

9. CONCLUSION

The work developed throughout this thesis aimed to provide solutions to fully control a quadcopter. Linear and nonlinear techniques were applied to tackle this problem, with different architectures being studied and devised for each technique. The developed strategies were all tested in simulation, which allowed to determine the most promising. The selected approaches were successfully validated in a commercially available quadcopter.

The control schemes devised demonstrated the capacity to seamlessly follow a predefined trajectory in the presence of measurement noises in simulation. Furthermore, in the robustness test to model parameters variation, the first architecture was able to meet the performance criteria when simultaneous variations of 50% in the mass and an increase of 300% in the inertia values were considered, which constitutes an interesting level of robustness for a linear approach. The nonlinear solution was capable of handling variations of 50% in the mass together with inertia values four times lower and four times higher than the value considered in the model without considerably affecting its responses.

Both control solutions were successfully implemented on an off-the-shelf quadrotor. The results obtained in trajectory tracking validated the proposed strategies and, given the manifest similarities between the attained responses with the actual aerial vehicle and in simulation, evidenced that the dynamical model considered, obtained resorting to the Newton-Euler formalism, is accurate and sufficient, even though higher order effects were neglected. The integrative action present in both architectures led to null steady-state position error, even when a heavier battery was used. The small angle approximation considered in the linearization of the dynamics was verified, which contributed to achieving good overall performance with the linear controller. Notwithstanding, the application of the static feedback linearization to the attitude and altitude dynamics improved the performance since the obtained position and yaw angle error was inferior compared with the obtained with the first solution. The highest root-mean-square error obtained with the linear approach was 0.1010 m, for the x inertial coordinate, and, with the nonlinear control scheme, was 0.0666 m, verified for the same coordinate. Moreover, the second control scheme originated an actuation with less variation than the first solution.

In summary, two different control solutions, using linear and nonlinear methods, capable of following a predefined trajectory and presenting null steady-state position error and a reasonable level of robustness to model imprecision, uncertainty and disturbances, were successfully devised, tested in simulation and validated in experimental tests resorting to a commercially available quadcopter.

10. ACKNOWLEDGEMENTS

This work was supported by FCT, through IDMEC, under LAETA, project UID/EMS/50022/2019.

REFERENCES

Bauer, P. and Bokor, J. (2008). Lq servo control design with kalman filter for a quadrotor uav. *Periodica Polytechnica Transportation Engineering*, 36(1-2), 9–14.

Bouabdallah, S., Noth, A., and Siegwart, R. (2004). Pid vs lq control techniques applied to an indoor micro quadrotor. *IEEE/RSJ International Conference on Intelligent Robots and Systems (IROS)*, 3, 2451–2456.

Das, A., Subbarao, K., and Lewis, F. (2008). Dynamic inversion of quadrotor with zero-dynamics stabilization. *2008 IEEE International Conference on Control Applications*.

Freddi, A., Lanzon, A., and Longhi, S. (2011). A feedback linearization approach to fault tolerance in quadrotor vehicles. *IFAC Proceedings Volumes*, 44(1), 5413–5418.

Henson, M. and Seborg, D.E. (1997). *Nonlinear process control*. Prentice Hall PTR.

Kalman, R.E. (1960). A new approach to linear filtering and prediction problems. *Journal of Basic Engineering*, 82(1), 35–45.

Lee, D. (2016). Ar.drone 2.0 support from embedded coder. URL `https://www.mathworks.com/hardware-support/ar-drone.html`.

Leishman, J.G. (2000). *Principles of helicopter aerodynamics*. Cambridge University Press.

Madeiras, J., Cardeira, C., and Oliveira, P. (2019). Complementary filter vision-aided for attitude and position estimation: Design, analysis and experimental validation.

Madgwick, S.O.H., Harrison, A.J.L., and Vaidyanathan, R. (2011). Estimation of imu and marg orientation using a gradient descent algorithm. In *2011 IEEE International Conference on Rehabilitation Robotics*, 1–7.

Mahony, R., Kumar, V., and Corke, P. (2012). Multirotor aerial vehicles: Modeling, estimation, and control of quadrotor. *IEEE Robotics Automation Magazine*, 19(3), 20–32.

Oriolo, G., Sciavicco, L., Siciliano, B., and Villani, L. (2010). *Robotics: Modelling, Planning and Control*. Springer.

Raja, M. (2017). *Extended Kalman Filter and LQR controller design for quadrotor UAVs*. Master's thesis, Wright state University, Dayton,Ohio.

Vepa, R. (2017). *Nonlinear Control of Robots and Unmanned Aerial Vehicles: an integrated approach*. CRC Press Taylor & Francis Group.

Wang, J., Bierling, T., Achtelik, M., Hocht, L., Holzapfel, F., Zhao, W., and Go, T.H. (2011). Attitude free position control of a quadcopter using dynamic inversion. *Infotech@Aerospace 2011*.